

# Propagation dynamics of optical vortices due to Gouy phase

S. M. Baumann, D. M. Kalb, L. H. MacMillan and E. J. Galvez

Department of Physics and Astronomy, Colgate University  
Hamilton, New York, 13346  
[egalvez@mail.colgate.edu](mailto:egalvez@mail.colgate.edu)

**Abstract:** We study the propagation of off-axis vortices in a paraxial beam formed by two collinear Laguerre-Gauss beams. We show that the vortices move about the beam axis as the light propagates resulting in a rotation of the beam's transverse profile. This rotation is explained by the Gouy phase acquired by the component beams. Experimental measurements of the angular position of the vortices are in good agreement with a two-mode theory.

© 2009 Optical Society of America

**OCIS codes:** (260.6042) Singular Optics; (050.4865) Optical Vortices.

---

## References and links

1. D. L. Andrews, *Structured Light and Its Applications: An Introduction to Phase-Structured Beams and Nanoscale Optical Forces*, (Academic Press-Elsevier, Burlington, 2008).
2. L. Allen, M. W. Beijersbergen, R. J. C. Spreeuw, and J. P. Woerdman, "Orbital angular momentum of light and the transformation of Laguerre-Gauss modes," *Phys. Rev. A* **92**, 8185–8189 (1992).
3. M. S. Soskin and M. V. Vasnetsov, "Singular Optics," in *Progress in Optics 42*, E. Wolf, ed. (Elsevier 2001), pp. 219–276.
4. G. Indebetow, "Optical vortices and their propagation," *J. Mod. Opt.* **40**, 73–87 (1993).
5. D. Rozas, C. T. Law, G. A. Swartzlander, Jr., "Propagation dynamics of optical vortices," *J. Opt. Soc. Am. B* **14**, 3054–3065 (1997).
6. M. V. Berry and M. R. Dennis "Knotted and linked phase singularities in monochromatic waves," *Proc. R. Soc. Lond. A* **457** 2251–2263 (2001).
7. M. V. Berry and M. R. Dennis "Knotting and unknotting of phase singularities: Helmholtz waves, paraxial waves and waves in 2+1 spacetime," *J. Phys. A* **34** 8877–8888 (2001).
8. J. Leach, M. R. Dennis, J. Courtial, and M. J. Padgett, "Vortex knots in light," *New J. Phys.* **7**, 1–11 (2005).
9. A. I. Bishop, T. A. Niemen, N. R. Heckenberg, and H. Rubinsztein-Dunlop, "Optical microrheology using rotating laser-trapped particles," *Phys. Rev. Lett.* **42**, 198104-1-4 (2004).
10. G. Molina-Terriza, J. P. Torres, L. Torner, "Management of the angular momentum of the light: preparation of photons in multidimensional vector states of angular momentum," *Phys. Rev. Lett.* **88**, 013601-1-4 (2002).
11. G. Gibson, J. Courtial, M. J. Padgett, M. Vasnetsov, V. Pas'ko, S. M. Barnett, and S. Franke-Arnold, "Free-space information transfer using light beams carrying orbital angular momentum," *Opt. Express* **12**, 5448–5456 (2004).
12. E. J. Galvez, N. Smiley, N. Fernandes, "Composite optical vortices formed by collinear Laguerre-Gauss beams," *Proc. SPIE* **6131**, 19–26 (2006).
13. E. J. Galvez and S. M. Baumann, "Composite vortex patterns formed by component light beams with non-integral topological charge," *Proc. SPIE* **6905**, 6905D-1-7 (2008).
14. S. Franke-Arnold, J. Leach, M. J. Padgett, V. E. Lembessis, D. Ellinas, A. J. Wright, J. M. Girkin, P. Ohberg, and A. S. Arnold, "Optical ferris wheel for ultracold atoms," *Opt. Express* **15**, 8619–8625 (2007).
15. C. R. Carpenter, "Gouy phase advance with microwaves," *Am. J. Phys.* **27**, 98–100 (1959).
16. J. H. Chow, G. de Vine, M. B. Gray, and D. E. McClelland, "Measurement of Gouy phase evolution by use of spatial mode interference," *Opt. Lett.* **29**, 2339–2341 (2004).
17. A. B. Ruffin, J. V. Rudd, J. F. Whitaker, S. Feng, and H. G. Winful, "Direct observation of the Gouy phase shift with single-cycle terahertz pulses," *Phys. Rev. Lett.* **83**, 3410–3413 (1999).
18. F. Lindner, G. G. Paulus, H. Walther, A. Baltuska, E. Goulielmakis, M. Lezius, and F. Krausz, "Gouy phase shift for few-cycle laser pulses," *Phys. Rev. Lett.* **92**, 113001-1–4 (2004).
19. J. Arlt, "Handedness and azimuthal energy flow of optical vortex beams," *J. Mod. Opt.* **50**, 1573–1580 (2003).

20. J. Hamazaki, Y. Mineta, K. Oka, and R. Morita, "Direct observation of Gouy phase shift in a propagating optical vortex," *Opt. Express* **14**, 8382–8392 (2006).
21. I. V. Basistiy, V. Yu. Bazhenov, N. S. Soskin, and M. V. Vasnetsov, "Optics of light beams with screw dislocations," *Opt. Commun.* **103**, 422–428 (1993).
22. S. M. Baumann and E. J. Galvez, "Non-integral vortex structures in diffracted light beams," *Proc. of SPIE* **6483**, 64830T-1-8 (2007).
23. M. W. Beijersbergen, L. Allen, H.E.L.O. van der Veen, and J. P. Woerdman, "Astigmatic laser mode converters and transfer of orbital angular momentum," *Opt. Commun.* **96**, 123–132 (1993).
24. N. R. Heckenberg, R. McDuff, C. P. Smith, H. Rubinztein-Dunlop, and M. J. Wegener, "Laser beams with phase singularities," *Opt. Quantum Electron.* **24**, 951-962 (1998).
25. M. W. Beijersbergen, R. P. C. Coerwinkel, M. Kristensen, and J. P. Woerdman, "Helical-wavefront laser beams produced with a spiral phase plate," *Opt. Commun.* **112**, 321–324 (1994).
26. I. D. Maleev and G. A. Swartzlander, Jr., "Composite optical vortices," *J. Opt. Soc. Am. B* **20**, 1169–1176 (2003).
27. D. M. Kalb and E. J. Galvez, "Composite vortices of displaced Laguerre-Gauss beams," *Proc. SPIE* **7227**, 72270B-1–8 (2009).
28. J. Courtial, "Self-imaging beams and the Gouy effect," *Opt. Commun.* **151**, 1–4 (1998).
29. K. Patorski, "The self-imaging phenomenon and its applications" in *Progress in Optics* 27, E. Wolf, ed. (1989) pp. 1–108.

---

## 1. Introduction

The study of optical singularities offers new insights into the free-space propagation of complex light forms. Optical singularities are unique and recognizable features that can be followed as the light propagates. The study of their evolution has led to a new view of wave-fields and their applications [1].

Of the many optical singularities exhibited by wave fields optical vortices are the most interesting and fundamental. These are singularities in the phase of the light and thus represent the *absence* of light. However, optical vortices are surrounded by a wave field whose phase advances around the vortex, and whose associated wavefront carries orbital angular momentum [1]. On-axis optical vortices, such as those carried by Laguerre-Gauss (LG) solutions of the paraxial wave equation in cylindrical coordinates [2], seem to possess a propagation invariance: they are always located on the beam axis. The phase around the vortex advances monotonically and linearly with the azimuthal coordinate completing whole multiples of  $2\pi$  in winding around the beam axis. However, on axis vortices are perhaps the exception to a general rule, in which the phase advances nonlinearly and where the vortices are not on the beam axis and move about it as the light propagates. These more general cases can be produced by superpositions of LG beams.

In recent years there has been much interest in optical vortex propagation, and in general, in the propagation of optical singularities [3]. From a fundamental perspective they enable the study of phase singularities in a more dynamical context [4, 5], where twists, loops and knots in the path of the vortices have been shown to appear [6, 7, 8]. The applications of optical vortices are intriguing and interesting, from the manipulation of objects in optical tweezers [9] to the encoding of information [10, 11].

In this article we study the simplest scenario of dynamical propagation of off-axis optical vortices. We will show that in composite beams formed by collinear superpositions of LG beams, off-axis vortices appear [12], and upon propagation these move about the beam axis consistent with a rotation of the beam profile. The motion of these off-axis (hereafter called peripheral) vortices can be well explained by the Gouy phase. This is the phase that a wave acquires as it changes its radius of curvature due to diffraction.

The above mentioned rotation of the beam can also be used as a new way to measure the Gouy phase. The Gouy phase of optical beams can be observed by interference: superposing a fundamental Gaussian beam going through a focal point with a plane wave [15]. The Gouy phase shift clearly manifests itself when few-cycle pulses go through a focal point [17, 18]. In

recent years high-order optical modes have been used to measure the Gouy phase. Basistiy et al. observed the angular motion of vortices generated by a binary grating containing two phase dislocations [21]. More recently Chow and coworkers made a precise measurement of the the Gouy phase via interference of fundamental and first-order Hermite Gauss modes [16]. The observed rotation of truncated beams with a definite high-order-mode helicity has also been linked to the Gouy phase [19, 20]. Our work in this article can be more closely connected to the work of Basistiy et al. [21], with the difference that we study the actual superposition of beams.

This article is divided as follows. In Sec. 2 of this article we summarize the resulting vortex patterns that are obtained when two collinear beams interfere. Then in Sec. 3 we discuss the propagation of these patterns and their connection to the Gouy phase.

## 2. Composite vortices

Recently we initiated the study of the pattern of vortices that arises in the collinear superposition of component LG beams with integral [1, 12] and non-integral [13] topological charges (see also Ref. [14] for related work). Below we give a summary of the results for integral vortices.

When two optical beams in LG eigenmodes are superimposed collinearly they generate a pattern of vortices that depends on the relative amplitude and phase of the component beams. LG modes have circular symmetry; a general LG mode has  $p$  radial nodes in its amplitude. In the present work we will limit ourselves to singly-ringed modes with  $p = 0$ . The amplitude of singly-ringed LG modes with topological charge  $\ell$  can be expressed as [2]

$$\mu^\ell = \left( \frac{2}{\pi|\ell|!} \right)^{1/2} \frac{1}{w} \left( \frac{r\sqrt{2}}{w} \right)^{|\ell|} e^{-r^2/w^2} e^{-i\ell\phi} e^{i[kz - kr^2/(2R)]} e^{i\varphi}, \quad (1)$$

where  $r$ ,  $\phi$  and  $z$  are the cylindrical coordinates,  $w$  is the beam radius,  $k$  is the wave number,  $R$  is the radius of curvature of the wave-front,  $\varphi = (N + 1) \tan^{-1}(z/z_R)$  is the Gouy phase, and  $z_R$  is the Raleigh range. The order  $N$  for a general LG mode is defined as  $N = 2p + |\ell|$ . Equation (1) represents a subset of the Laguerre-Gauss family of modes that has a distinct intensity profile consisting of single a ring, or “doughnut.” At the center of the ring is a phase vortex of topological charge  $\ell$ . The radius of the ring, defined by the distance from the center to points where the intensity is maximum is given by

$$\rho = \sqrt{\frac{\ell}{2}} w. \quad (2)$$

Consider now the superposition of two collinear component beams with topological charges  $\ell_1$  and  $\ell_2$ . The total amplitude can be expressed as

$$\mu_T = \sin \theta \mu^{\ell_1} + \cos \theta \mu^{\ell_2} e^{i\delta}, \quad (3)$$

where  $\delta$  is the relative phase between the two beams. The ratio of the amplitudes of the two component beams is specified by

$$\alpha = \sqrt{\frac{I_1}{I_2}} = \tan \theta, \quad (4)$$

where  $I_1$  and  $I_2$  are the component-beam intensities. There are two distinct cases of beams created in this way.

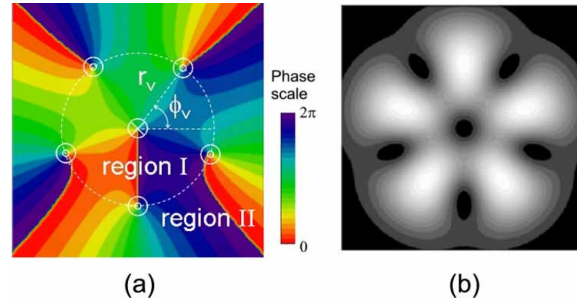


Fig. 1. Numerical calculation of the composite-vortex pattern generated by combining two Laguerre-Gauss beams with  $\ell_1 = -1$  and  $\ell_2 = +4$ . In (a) the computed composite vortex pattern can be viewed by the color-encoded phase map of the light pattern. Circular symbols denote the position of the vortices, where a positive charge denotes a counter-clockwise increase in the phase. The intensity pattern is shown in (b) in grey scale.

### 2.1. Case $|\ell_1| < |\ell_2|$

The resulting composite-vortex beam has a very characteristic form, shown in the phase map of Fig. 1(a). It contains a vortex of charge  $\ell_1$  in the center of the beam surrounded by  $|\ell_1 - \ell_2|$  singly charged peripheral vortices of sign  $\sigma_2 = \ell_2/|\ell_2|$  located at the same radial distance

$$r_v = \frac{w}{\sqrt{2}} \left( \frac{|\ell_2|!}{|\ell_1|!} \alpha^2 \right)^{\frac{1}{2(|\ell_2| - |\ell_1|)}} \quad (5)$$

from the center of the beam. These vortices are evenly distributed at angles

$$\phi_v = \frac{\delta + n\pi}{\ell_2 - \ell_1}, \quad (6)$$

where  $n = 1 \dots (2|\ell_1 - \ell_2| - 1)$  is an odd integer for each of the peripheral vortices. This pattern of vortices arises because the intensity radii of two modes is different (i.e., see Eq. (2)). The shear in the phase of the two modes located at different radii creates the peripheral vortices. To understand this consider the case where the amplitudes of the component beams are the same:  $\alpha = 1$ . The inner region I is dominated by the beam with  $\ell_1$ , where  $|\mu^{\ell_1}| > |\mu^{\ell_2}|$ , and conversely, the outer region II is dominated by the beam with  $\ell_2$  (i.e. where  $|\mu^{\ell_1}| < |\mu^{\ell_2}|$ ). The boundary between the two regions is a circle of radius  $r_v$ . That is, the peripheral vortices are located precisely at the boundary region of intensity dominance of the two modes.

The vortices are located at the angles  $\phi_v$  where phases of the dominant modes  $\ell_1 \phi_v$  and  $\ell_2 \phi_v$  at each side of the boundary differ by an odd multiple of  $\pi$ . Indeed it is trivial to show that Eq. (6) arises from  $\ell_2 \phi_v - \ell_1 \phi_v - \delta = n\pi$ . Figure 1(a) shows the computed phase of the composite vortex pattern for the case where  $\ell_1 = -1$  and  $\ell_2 = +4$ . The adjacent figure shows a computation of the corresponding intensity pattern.

In the laboratory we can vary two parameters: the relative amplitude of the two beams  $\alpha$  and the phase between them  $\delta$ . As  $\alpha$  is varied the boundary between regions I and II changes and consequently the peripheral vortices move radially in(out) as  $\alpha$  decreases(increases).

We studied this in the laboratory using the setup shown in Fig. 2. Light from a HeNe laser was sent to two nested Mach-Zehnder interferometers. Light going through one of the arms of the outer interferometer was expanded and used as a reference beam. With this beam we created fringe interference patterns with the composite beam that allowed us to locate the vortices. Light going through the other outer arm went to an inner interferometer. This interferometer

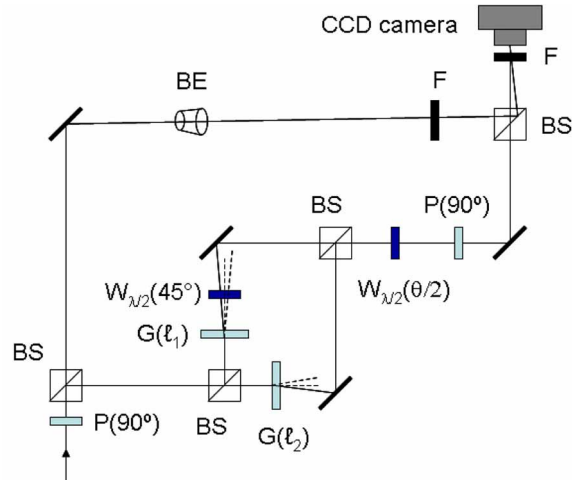


Fig. 2. Schematic of the apparatus used to study composite vortices. Polarizers [ $P(\alpha)$ ] and half-wave plates [ $W_{\lambda/2}(\alpha)$ ] oriented an angle  $\alpha$  relative to the horizontal are used to control the relative intensity of the interfering beams. Two forked binary gratings [ $G(\ell)$ ] of charge  $\ell$  are used to prepare the component beams. A beam expander ( $BE$ ) and neutral density filter ( $F$ ) are used to prepare a reference beam. Non-polarizing beams splitters ( $BS$ ) are used to split and combine the light.

was used to prepare the composite beam via forked binary gratings  $G(\ell)$  of topological charge  $\ell$  located past the output ports of the first beam splitter. Mirrors following the gratings steered the light to the second beam splitter. One of the mirrors was mounted on a translation stage with a piezo-electric ceramic placed as a spacer. By applying a voltage to the piezo-electric element we were able to adjust the phase  $\delta$  between the two interfering modes.

The ratio of amplitudes  $\alpha$  was adjusted via the polarization of the light [12, 13]. The light entering the interferometer was linearly polarized in the vertical plane. A half-wave plate  $W_{\lambda/2}(45^\circ)$  with its fast axis forming an angle of  $45^\circ$  with the horizontal was placed in one of the arms of the interferometer to rotate the plane of polarization of the light to the horizontal plane. Thus, the two beams emerged from the interferometer with orthogonal polarizations. After the interferometer we had a half-wave plate ( $W_{\lambda}(\theta/2)$ ) with its fast axis oriented at an angle  $\theta/2$  relative to the horizontal followed by a polarizer with its transmission axis along the vertical direction. This arrangement allowed us to set the intensity ratio via the setting of  $\theta$  and Eq. (4).

The composite beam was steered to a charge-coupled-device (CCD) camera where it interfered with the expanded reference beam. The top two rows of Fig. 3 show false-color interferograms of the composite beams corresponding to  $\ell_1 = -1$  and  $\ell_2 = +4$ . Careful inspection of the figures reveals the presence forks in each of the dark regions. (Per the preceding discussion, we have a vortex with charge  $-1$  in the center of the beam, and five vortices of charge  $+1$  distributed symmetrically in the periphery.) The vortices are located at the fork dislocations in the fringe interference pattern of Fig. 3. The first row of frames shows interferograms for several values of  $\theta = \tan^{-1} \alpha$  in increments of  $\pi/8$  but with a fixed value of  $\delta$ . The left most frame, which corresponds to the case  $\theta = 0$ , consists of a purely  $\ell_2 = +4$  beam; the middle frame corresponds to the case  $\theta = \pi/4$  (i.e., equal component-beam amplitudes), and the right-most frame corresponds to the case  $\theta = \pi/2$ , where the beam is purely the  $\ell_1 = -1$  component. It can be seen that the peripheral vortices move outwards as  $\theta$  is increased. Notice that the tines of

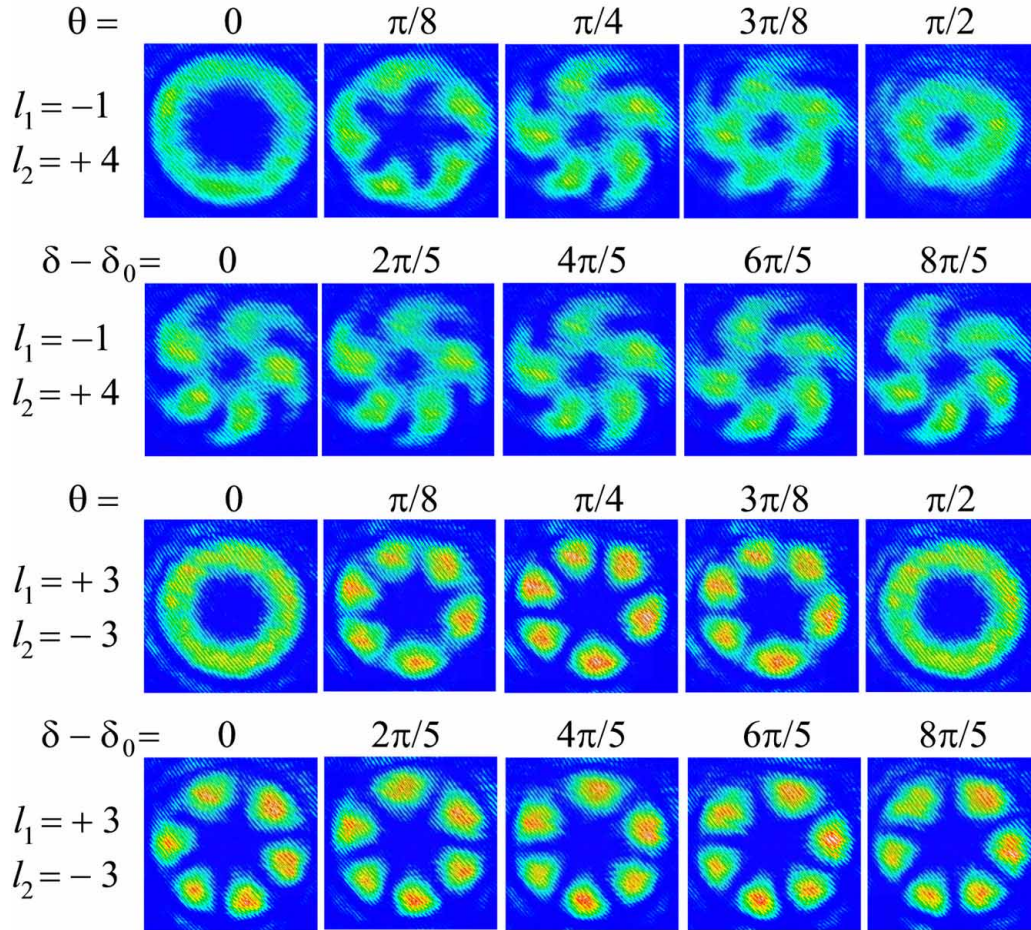


Fig. 3. Image of composite beam patterns as a function of experimental parameters. The first row and (Media 1) show the composite beam as a function of the relative amplitude  $\alpha$  of the component beams with  $\ell_1 = -1$  and  $\ell_2 = +4$ .  $\alpha$  is specified by the  $\theta$  via  $\alpha = \tan \theta$ . The second row and (Media 2) show the composite as a function of the relative phase  $\delta$  of the component beams with  $\ell_1 = -1$  and  $\ell_2 = +4$ , and  $\alpha = 1$ . The third row and (Media 3) show the composite beam as a function of  $\theta$  for  $\ell_1 = +3$  and  $\ell_2 = -3$ . The fourth row and (Media 4) show the composite beam as a function of  $\delta$  for  $\ell_1 = +3$  and  $\ell_2 = -3$ , and  $\alpha = 1$ .

the central and peripheral forks point in opposite directions. This denotes their opposite charge [22]. The curving of the intensity lobes is due to slight differences in the radii of curvature between the component beams. The accompanying video (Media 1) shows a more complete sequence: the radial motion of the peripheral vortices for a continuous change in  $\theta$ .

The set of frames in the second row of Fig. 3 shows the composite pattern as  $\delta$  is changed while  $\alpha$  is kept fixed at 1. Following Eq. (6), if we increase  $\delta$  by  $\Delta\delta$  the pattern will rotate by  $\Delta\phi_r = \Delta\delta/(\ell_2 - \ell_1)$ . Thus, for the case of the figure ( $\ell_1 = -1$  and  $\ell_2 = +4$ ), a change in phase by  $\Delta\delta = 2\pi$  corresponds to a rotation of the composite by  $2\pi/5$  or  $72^\circ$ . An accompanying video (Media 2) shows the motion of the pattern for a continuous change in the phase delta. (The initial phase in the video was set to zero for labeling convenience.) The rotation of the

peripheral vortices about the center of the beam has been referred to as the “optical Ferris wheel” [14].

## 2.2. Case $\ell_1 = -\ell_2$

This second case is unique because it is an exception to the general case: the composite beam contains no peripheral vortices for any of the relevant parameters. When  $\alpha = 1$  there are  $2|\ell_1|$  angular nodes symmetrically distributed about the beam axis at angles  $\phi_s = \phi_v$ , where  $\phi_v$  is given by Eq. (6). At the nodes we have shear phase singularities, where the phase abruptly switches by  $\pi$ . For cases where  $\ell_1$  is 1 and 2 the resulting modes are the Hermite-Gauss modes  $HG_{01}$  (or  $HG_{10}$ ) and  $HG_{11}$ , respectively [23]. For higher orders, the resulting patterns are no longer Hermite-Gauss eigenmodes. When the amplitudes of the component beams are not the same the phase at the nodes varies continuously. In these cases the center of the beam contains a vortex with the same charge as the beam with the greater amplitude. Computer simulations that we have done show that the rate of change of the phase decreases as  $\alpha$  varies away from 1.

The third and fourth rows of Fig. 3 show the composite pattern when  $\ell_1 = 3$ . In the third row  $\theta$  is changed in increments of  $\pi/8$  while keeping  $\delta$  fixed. The left-most and right-most frames are the beams with  $\ell_2 = -3$  and  $\ell_1 = +3$ , respectively. In the middle frame both component beams have equal amplitude. One can see the  $\pi$  phase difference between adjacent lobes by the discontinuous shift in the fringes from lobe to lobe. The fourth row shows composite beams taken for different values of  $\delta$  in increments of  $2\pi/5$  for  $\alpha = 1$ . Following an argument similar the previous case, we can see that the rotation of the pattern follows  $\delta/2\ell_2$ . Accompanying videos, (Media 3) and (Media 4), show the same patterns for continuous change of  $\theta$  and  $\delta$ , respectively.

## 3. Gouy rotation

The previous results present symmetrical patterns in light beams that rotate as the dynamical phase between the component beams is varied. These are patterns that can be seen on a screen or camera placed in the path of the light. In general these patterns rotate about the beam axis as the beam propagates. This occurs via the Gouy phase difference between the component beams.

The Gouy phase for LG beams of topological charge  $\ell$  and radial mode  $p$  is given by

$$\varphi = (2p + |\ell| + 1)\xi, \quad (7)$$

where  $\xi = \tan^{-1}(z/z_R)$  with  $z_R$  being the Raleigh range.

When accounting for the Gouy phase of singly-ringed (i.e.,  $p = 0$ ) component beams the angular position of the peripheral vortices is

$$\phi_v = \frac{\delta + n\pi + (|\ell_2| - |\ell_1|)\xi}{\ell_2 - \ell_1}. \quad (8)$$

If we maintain the dynamic phase  $\delta$  constant, the angular change in the vortex position between two points along the beam propagation direction is

$$\Delta\phi_v = \frac{|\ell_2| - |\ell_1|}{\ell_2 - \ell_1} \Delta\xi \quad (9)$$

We can subdivide this situation into three cases. Case (i) is when  $|\ell_1| \neq |\ell_2|$  and  $\sigma_1 = \sigma_2$ . In this case

$$\Delta\phi_v = \sigma_2 \Delta\xi. \quad (10)$$

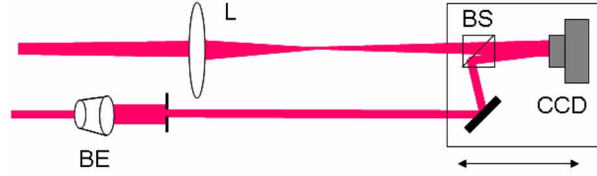


Fig. 4. Schematic of the section of the apparatus used to measure the rotation of the beam as a function of the propagation distance. The composite beam is focused by a lens ( $L$ ). A reference beam is expanded by a beam expander ( $BE$ ) and combined with the composite beam via a beam splitter ( $BS$ ) so to form a fringe pattern on the CCD camera.

Case (ii) is when  $|\ell_1| \neq |\ell_2|$  and  $\sigma_1 = -\sigma_2$ , which results in

$$\Delta\phi_v = \frac{|\ell_2| - |\ell_1|}{|\ell_2| + |\ell_1|} \sigma_2 \Delta\xi. \quad (11)$$

This case reduces to the previous one when  $\ell_1 = 0$ . The maximum rotation of the beam is  $\pi$  when  $\Delta\xi = \pi$ . In this second case the rotation reduces as  $|\ell_1|$  increases up to  $|\ell_2|$ . Case (iii) is the limiting case, where  $|\ell_1| = |\ell_2|$ . In this case there is no rotation:

$$\Delta\phi_v = 0. \quad (12)$$

For case (i) the combination of the angular rotation of the vortices and the expansion of the beam due to diffraction leads to straight-line trajectories in three dimensional space. This is due to the  $z$ -dependence of the radial and angular position of the vortices, given by  $r_v \propto w$  with  $w = w_0(1 + z^2/z_R^2)$  (see Eq. (5);  $w_0$  is the waist) and  $\tan\Delta\phi_v = \pm z/z_R$  (see Eq. (10)), respectively. This type of vortex trajectory was studied analytically and numerically in Ref. [5] for two situations that fall under case (i), but using a model that consists of the product of a vortex function with a Gaussian background [4]. However, for case (ii) above the vortices do not describe such straight-line trajectories. This is because  $\tan\Delta\phi_v \neq \pm z/z_R$ . Instead they describe trajectories that are twisted hyperbolas of shape that depend on the relation between  $\Delta\phi_v$  and  $\Delta\xi$  in Eq. (11).

We made detailed measurements of the beam rotation for the case where  $\ell_1 = 0$  and  $\ell_2 = 2$ . This case is most suited for our purpose since it has two peripheral vortices on opposite sides of the beam axis and with no central vortex. Thus, the line joining the two vortices serves to measure the rotation of the beam. This is also a case where the composite beam achieves the maximum rotation. The apparatus that we used to do these measurements is shown in Fig. 4. We used a 1-m focal length lens to focus the light, and imaged the beam pattern along the propagation direction with a CCD camera mounted on a plate sitting on an optical rail. Also mounted on the plate where a mirror and beam-splitter. They were used to send an expanded reference beam also to the camera for producing interferograms. We located the vortices via the forks in the interferograms—we found that the use of the dark regions of the composite pattern unreliable for this purpose. The orientation of the line joining the vortices was used as a measure of the beam rotation.

Figure 5 shows our data taken for the range of values of  $z$  accessible to us. The function  $\Delta\phi_F \tan[(z - z_0)/z_R] + \Delta\phi_0$  was fit to the data. We obtained  $\Delta\phi_F = (0.98_{-0.21}^{+0.37})\pi$  in excellent agreement with the expectation, i.e.,  $\pi$ . The fitted values of the other parameters were  $z_0 = 127 \pm 10$  cm,  $z_R = 23 \pm 14$  cm and  $\Delta\phi_0 = -53^\circ$ . These have been incorporated into the graph so that we can better appreciate it. The inserts show interferograms taken along the way, displaying the rotation of the beam as the light goes through the focal point. The intensity of the light in

the frames was adjusted to avoid saturating the CCD camera. We took several data sets like the ones shown in the figure.

While the data of Fig. 5 shows reasonable agreement with the expected Gouy phase shift, it does not perfectly follow the theoretical curve for values of  $(z - z_0)/z_R$  beyond 1. We noticed that for those values the shape of the beam also changed from a well defined ring to a broader one. As a consequence the radial position of the vortices was not as expected, but closer to the beam axis. This may be due to small contributions of modes with  $\ell = 2$  and  $p > 0$  present in the beam. These modes arise from the lack of purity in the mode generated by the first-order diffraction of a zero-order Gaussian beam from the binary forked grating [24, 25]. As the beam propagates through the focal point, the rephasing of these modes, which have a different Gouy phases, may alter the shape of the beam and the location of the vortices, not accounted by the two-mode theoretical curve.

We also tested the predictions for a variety of values of  $\ell_1$  and  $\ell_2$ . Figure 6 shows two cases taken with a slightly different setup. The composite beams were prepared with the setup of Fig. 2. The component beams had equal amplitudes (i.e.,  $\alpha = 1$ ). The composite beam was then sent to a lens with a focal length  $f = 2.44\text{m}$ . The beam past the lens focused with a Rayleigh range  $z_R = 0.657\text{m}$ . We recorded images only from  $z = -z_R$  to  $z = +z_R$ , which amounted to  $\Delta\xi = \pi/2$  for that interval. The first row of Fig. 6 corresponds to  $\ell_1 = -2$  and  $\ell_2 = +4$ . In these composite beams there are six peripheral vortices in between the “petals” of the pattern. The observed rotation is  $\Delta\phi_v = \pi/6$ , in agreement with the prediction given by Eq. (11) for  $\Delta\xi = \pi/2$ . (The direction of rotation of the imaged pattern differs from previous ones due to an extra mirror in the setup.) The image rotated in the opposite direction when the signs of the charges were reversed.

The set of images in the second row of Fig. 6 correspond to the case where  $\ell_1 = 2$  and  $\ell_2 = -2$ . We observe no rotation, as predicted by the theory. This is because both component beams get the same Gouy phase (see Eq. (12)). This is also a case where the composite beam exhibits no peripheral vortices.

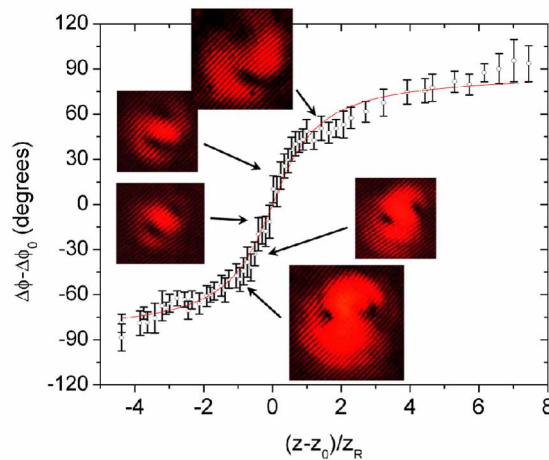


Fig. 5. Graph of the data taken with the setup of Fig. 4. It corresponds to the rotation of the beam with two peripheral vortices created by the superposition of  $\ell_1 = 0$  and  $\ell = 2$  modes as a function of propagation distance when the light goes through a focal point. The vortices were located by the forks in the interferograms of the composite beam. Inserts show samples of the beam at different locations.

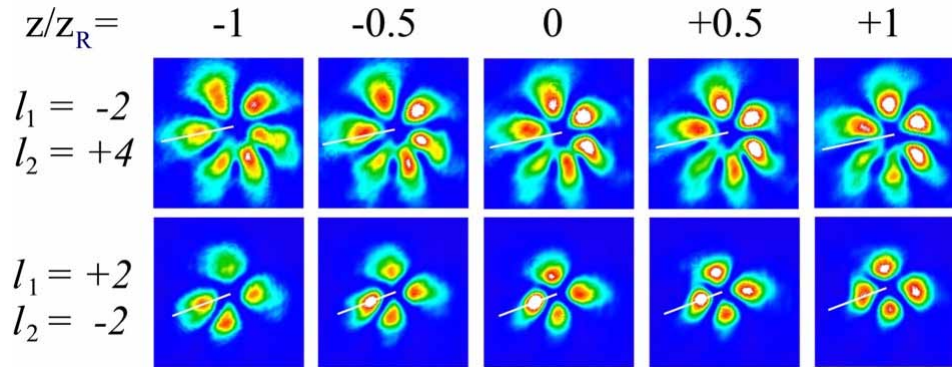


Fig. 6. Images testing the predictions for the rotation of the beam profiles as the light went through a focal point. The top row corresponds to a case where  $|\ell_1| \neq |\ell_2|$ , while the second row corresponds to the case where  $\ell_1 = -\ell_2$ .

#### 4. Discussion

In summary, we have shown that off axis optical vortices formed by collinear superpositions of LG beams move about the beam axis consistent with a rotation of the beam as it propagates. The amount of rotation is in agreement with the rephasing of the wavefront of the component beams due to Gouy phase. The results are also used as a measurement of the expected relative Gouy phase of the component beams. The sense of rotation of the beam is determined by the sign of the topological charge with largest magnitude.

In this study we have only considered collinear beams. When the beams are non-collinear a much more complicated situation arises [26, 27]. This is because the beam displacement breaks the cylindrical symmetry.

The composite beams that we have studied are part of a family of beams called “spiral-type” for  $|\ell_1| \neq |\ell_2|$  and “structurally stable” for  $|\ell_1| = |\ell_2|$  [28]. In these cases, besides from a change in size of the beam, the intensity pattern of the beam is preserved upon propagation, twisting as in the former case, or remaining constant for the latter case. It is interesting to inquire about the propagation of more than two modes. For more than two modes more interesting effects arise, such as the self-imaging or Talbot effect [28, 29], where the intensity pattern changes upon propagation, but undergoes a series of self-imaging revivals at periodic intervals. What is interesting is that a net chirality in the mode composition manifests as a rotation of the pattern in the revivals [28]. Indeed, even when the mode composition is infinite, a net chirality manifests in a rotation of the overall pattern [19, 20]. However, the trail of singularities for more than two component beams has yet to be investigated thoroughly, as knots and loops in the vortex trajectories [6, 7, 8] are a glimpse of their rich propagation dynamics.

#### Acknowledgments

This work was supported by a grant from Research Corporation. We also thank N. Fernandes, M. Novenstern, and N. Smiley for their early contributions and P. Crotty and J. Noé for help and useful discussions.